Environ Geochem Health
https://doi.org/10.1007/s10653-020-00566-7

ORIGINAL PAPER

Chromium, manganese, nickel, and cobalt mobility and bioavailability from mafic-to-ultramafic mine spoil weathering in western Massachusetts, USA

Justin A. Mistikawy · Trevor J. Mackowiak · Mark J. Butler · Ivan C. Mischenko · Richard S. Cernak Sr. · Justin B. Richardson

Received: 18 November 2019 / Accepted: 10 April 2020

Abstract Fragmented ultramafic bodies in New England were important mineral resources until the early twentieth century, yet few studies have addressed their potential to release trace metals to terrestrial and aquatic environments. Here, we evaluate the release of four trace metals (Cr, Co, Mn, and Ni) from a historic serpentine–talc "soapstone" quarry in Blandford, MA, USA. Soil pits, sediment and rock samples, and stream water samples were collected from upslope undisturbed areas, within the mine spoils and mine face, and downslope of the mine. In order to provide a bottom-up approach for understanding metal release, careful petrographic analysis, electron-dispersive spectroscopy, and wavelength-dispersive spectroscopy were employed to provide first-order insight into the mineralogy of the deposit and a determination of potential metal-bearing phases. Trace metals were primarily observed in ultramafic sheet silicates, primary Fe-oxides, and interstitial weathering-related sulfates. Bulk rock concentrations were Cr (1550 mg kg^{-1}), Co (230 mg kg^{-1}), Mn (1100 mg kg^{-1}), and Ni (1960 mg kg^{1}); Cr, Co, and Ni were elevated relative to the surrounding country rock. However, soils and sediments total concentrations were comparable to background soil concentrations: Cr (119 mg kg^{-1}), Co (73 mg kg^{-1}), Mn (894 mg kg^{-1}), and Ni (65 mg kg^{-1}). Moreover, $< 0.5\%$ of the total concentrations were bioavailable (0.1 M ammonium acetate extraction), implying that metals are present as insoluble forms. However, $\sim$ 20% of the total Cr, Mn, Ni, and Co concentrations were strong acid extractable, suggesting mobilization over the coming decades. Stream water concentrations of Mn and Cr were < 50 μg L^{-1}, below concentrations outlined by USEPA drinking water standards, and WHO water guidelines for Ni. These results suggest that transport of Cr, Mn, Ni, and Co from the serpentine–talc as dissolved compounds or sediments is limited by retention within silicate and oxides.

Keywords Biogeochemistry · Serpentine soils · Ecotoxicology · Mine tailings · Trace metals

Introduction

Ultramafic bodies constitute less than 1% of all terrestrially exposed rocks (Oze et al. 2007), yet their weathering demands interest due to the potential release of asbestos and excessive trace metals,

Electronic supplementary material The online version of this article (https://doi.org/10.1007/s10653-020-00566-7) contains supplementary material, which is available to authorized users.

J. A. Mistikawy · T. J. Mackowiak · M. J. Butler · I. C. Mischenko · R. S. Cernak Sr. · J. B. Richardson (✉)
Department of Geosciences, University of Massachusetts, 611 North Pleasant Street, Amherst, MA 01003, USA
e-mail: Jbrichardson@umass.edu

Published online: 25 April 2020

including chromium (Cr), manganese (Mn), nickel (Ni), and cobalt (Co), to the environment. The mobilization of these metals poses large threats to both terrestrial and aquatic ecosystems; toxic ions such as Ni and Cr^{VI} are abundant in mining spoils and pose great risk to surrounding soil and water ecosystems (Raous et al. 2013). Understanding the interplay between primary ultramafic mineralogy and chemical alteration/transport in the context of regional hydrological dynamics and biogeochemical cycling is critical for establishing chemical transport pathways and determining whether or not soils and water supplies are at risk of metal contamination from surrounding mining spoils.

Economically viable metal deposits hosted in highly altered ultramafic bodies are known as laterites and are well-documented in tropical climates including Brazil, India, and the Dominican Republic (Proenza et al. 2008). Although New England lacks high-grade deposits of this nature, ultramafic rocks are widely recognized across the region (Bradley 1983; Zen et al. 1983; Tracy et al. 1984; Jordan et al. 2019). The historically mined Osborne Quarry in Blandford, MA, is a small exposure of Ordovician mafic-to-ultramafic crust. The weathering of the rocks exposed in this historic quarry may serve as a significant source of metals to the nearby Cobble Mountain Reservoir, a major supply of freshwater to more than 200,000 residents of Massachusetts.

Chromium and Mn exist within silicate minerals due to substitutions for Mg or Fe, causing typical crustal rocks to have bulk concentrations ranging from 5 to 120 ppm (Adriano 2001). Common Cr-incorporating crustal minerals include chlorite (3000 mg kg^{-1}), enstatite (4000 mg kg^{-1}), actinolite (1000 mg kg^{-1}), augite (7000 mg kg^{-1}), magnetite (8200 mg kg^{-1}), and spinels (13,300 mg kg^{-1}) (Schwertmann and Latham 1986; Oze et al. 2004; Izbicki et al 2008). Common Cr-bearing minerals present in ultramafic and serpentinized rocks include chromite ($FeCr_2O_4$) or more complex non-silicate phases such as vauquelinite ($CuPb_2CrO_4$-PO_4OH), bentorite ($Ca_6(CrAl)_2(SO_4)_3$), and crocoite ($PbCrO_4$) (Avudainayagam et al. 2003; Babula et al. 2008). The most abundant Mn-bearing minerals in terrestrial systems are ferromagnesian silicates with minor Mn substitutions, such as olivine, pyroxene, biotite, and chlorite with Mn concentrations ranging from 10 to 14,000 mg kg^{-1}. Mn can also substitute in Ca-bearing aluminosilicates (felsic), like feldspars and muscovite with concentrations ranging from 4 to 400 mg kg^{-1}. Manganese may be present in parent in rocks as Mn-oxide minerals such as pyrolusite (MnO_2), braunite ($(Mn^{2+}Mn^{3+})_6(SiO_{12})$, and psilomelane ($(Ba, H_2O)_2$-$Mn_5O_{10}$) (Adriano 2001; Kabata-Pendias and Mukherjee 2007). The Osborne locality provides a unique opportunity to characterize the weathering of Fe–Mg-rich ultramafic lithologies in temperate climates while assessing water quality vulnerability in the context of historic mine metal drainage.

The USEPA has primary drinking water guidelines on Cr in drinking waters (100 µg L^{-1} USEPA 2019a, b). Chromium, especially Cr(VI), can negatively impact plants, terrestrial animals, and aquatic organisms (Singh et al. 2013). Manganese is an essential component of enzymes and proteins in mitochondria, Golgi bodies, and chloroplasts (da Silva and Williams 2001). High concentrations of Mn can cause imbalances of other metal nutrients within plant cells, especially in relation to Mg, Ca, and Zn (Cenni et al. 1998; de Varennes et al. 2001). The EPA has a secondary drinking water guideline for Mn of 50 µg L^{-1} (USEPA 2019a, b) for aesthetic purposes, but overexposure to Mn by children is receiving growing attention because of its role as a potential neurotoxin (e.g., Haynes et al. 2015).

Nickel and Co are commonly associated with primary and secondary phyllosilicates, especially serpentine, talc, and chlorite and sometimes Fe-rich silicates, e.g., olivine, pyroxene, and hornblende (Ratié et al. 2015). Cobalt is siderophilic and found in S-bearing rocks as sulfidic minerals such as cobaltite (CoAsS). Nickel can be both siderophilic or chalcophilic, substituting for Fe in minerals such as pentlandite ($(Ni,Fe)_9S_8$ or millerite (NiS) (Kabata-Pendias and Mukherjee 2007). Nickel is required for several essential enzymes in plants and animals, but overexposure can be toxic. The average Ni soil concentration globally and for the USA is 20 mg kg^{-1} (Adriano 2001). The World Health Organization has set a drinking water guideline for Ni at 70 µg L^{-1} (WHO 2017). Nickel soil concentrations of 10 to 100 mg kg^{-1} have been shown to be toxic to plants, but certain species can be more sensitive, with common tree genera such as *Picea*, *Larix*, and *Pinus* expressing toxicity at 1 to 10 mg kg^{-1} (Gasser et al. 1995). Although there are no drinking water guidelines for Co, overexposure can be toxic to plants and

humans (e.g., Adriano 2001; Li et al. 2009; Leyssens et al. 2017). Ecotoxicological effects on plants from Ni and Co due to serpentine and ultramafic weathering are commonly compounded or misconstrued due to co-occurrence of Ca deficiencies and excessive Mg or other toxic metals (Rabenhorst et al. 1982).

The objective of this study was to assess potential links between ultramafic weathering and Cr, Ni, Co, and Mn mobility/bioavailability in the rock, sediments, and soils surrounding the former Osborne Soapstone Quarry, Blandford, Massachusetts. Mining at Osborne ceased by the 1920s, but ultramafic mine spoils and exposed mining faces may be a significant source of trace metals to the environment, specifically through the breakdown of primary oxide and Fe–Mg-rich silicate phases. The goals of this study are twofold: (1) to determine trace metal host minerals in mined mafic-to-ultramafic rocks and spoils and (2) to determine the mobility and bioavailability of Cr, Mn, Ni, and Co with comparisons of total and bioavailable concentrations in upslope, within mine, and downslope of the mine soils, sediments, and stream waters draining from the mine area. We hypothesized that the ultramafic rocks are enriched in trace metals that could become bioavailable or easily mobilized. Furthermore, we hypothesized that soils derived from mine spoils and below the mine may be enriched in trace metals from the ultramafic portion of the deposit. Integrating mineralogical observation and quantitative constraints of mobile and bioavailable trace metals allows for understanding chemical alteration, susceptibility to metal leaching, and the potential impact of ultramafic and historic mines on an important body of drinking water in western Massachusetts.

Background, materials, and methods

Geologic background of the Osborne Mine

The Cobble Mountain Reservoir contains an estimated 22.8 billion gallons of water and is the primary freshwater supply of Springfield, MA (population 155,032 in 2019, US Census Bureau 2019). The reservoir is located in the township of Blandford, MA, and is situated within a steep, well-drained terrain underlain by compositionally variable crystalline bedrock (Fig. 1a). The reservoir is spatially associated with sulfidic schist, quartzite, amphibolite, and dispersed intrusive bodies associated with the Williamsburg granodiorite–pegmatite (Fig. 1b, Chute 1969). These lithologies belong to a number of geologic formations ranging in age from late Precambrian to Devonian and are well-described in central Massachusetts and across New England (Tracy et al. 1984; Zen et al. 1983). The middle Ordovician Ammonoosuc Volcanics, Partridge Formation, Chester Amphibolite, and Cobble Mountain Formation are known to outcrop by the reservoir and locally expose slivers of mafic-to-ultramafic crust (Chute 1969). Structural observation and petrogenetic analyses support interpretations that these mafic-to-ultramafic lenses originated as extensive lateral horizons during voluminous igneous emplacement related to the Devonian Acadian Orogeny (Tracy et al. 1984; Bradley 1983). Active prospecting and sporadic mining occurred at several of these localities from 1830 to 1912 throughout Massachusetts (Chute 1969; Bradley 1983; Zen et al. 1983; Tracy et al. 1984).

The former Osborne Quarry is located just uphill of the northern branch of the Cobble Mountain Reservoir in southeastern Blandford, MA (Fig. 1c). Commercial soapstone mining occurred intermittently at Osborne from 1830 to 1920 (Hitchcock 1833; Emerson 1898; Chute 1969). The deposit is structurally layered and steeply dips along the regional northwest-north strike (310, 62) within confining pelitic schist of the Cobble Mountain Formation and Chester Amphibolite (Chute 1969). The primary mining pit exposes a 3–5 m-thick deposit of massive serpentine–talc, or soapstone, up to 10 m in width. This central ultramafic zone is bounded by thin layers (3–8 m) of compositionally variable mafic schist along strike for approximately 70 m (Fig. 1d). Several small channels and streams that ultimately drain into the Cobble Mountain Reservoir flow through the main excavation pit and the large pile of mining spoils and talus adjacent to it. The weathering of mafic-to-ultramafic minerals and, moreover, mining spoils in the former Osborne Soapstone Quarry may therefore exert a strong control on the local trace metal chemistry of the Cobble Mountain Reservoir and its surrounding soils.

Rock, soil, sediment, and water sampling

Assessing the role of mafic-to-ultramafic weathering and metal mobility at the Osborne Quarry requires an understanding of the exposed lithology. There are

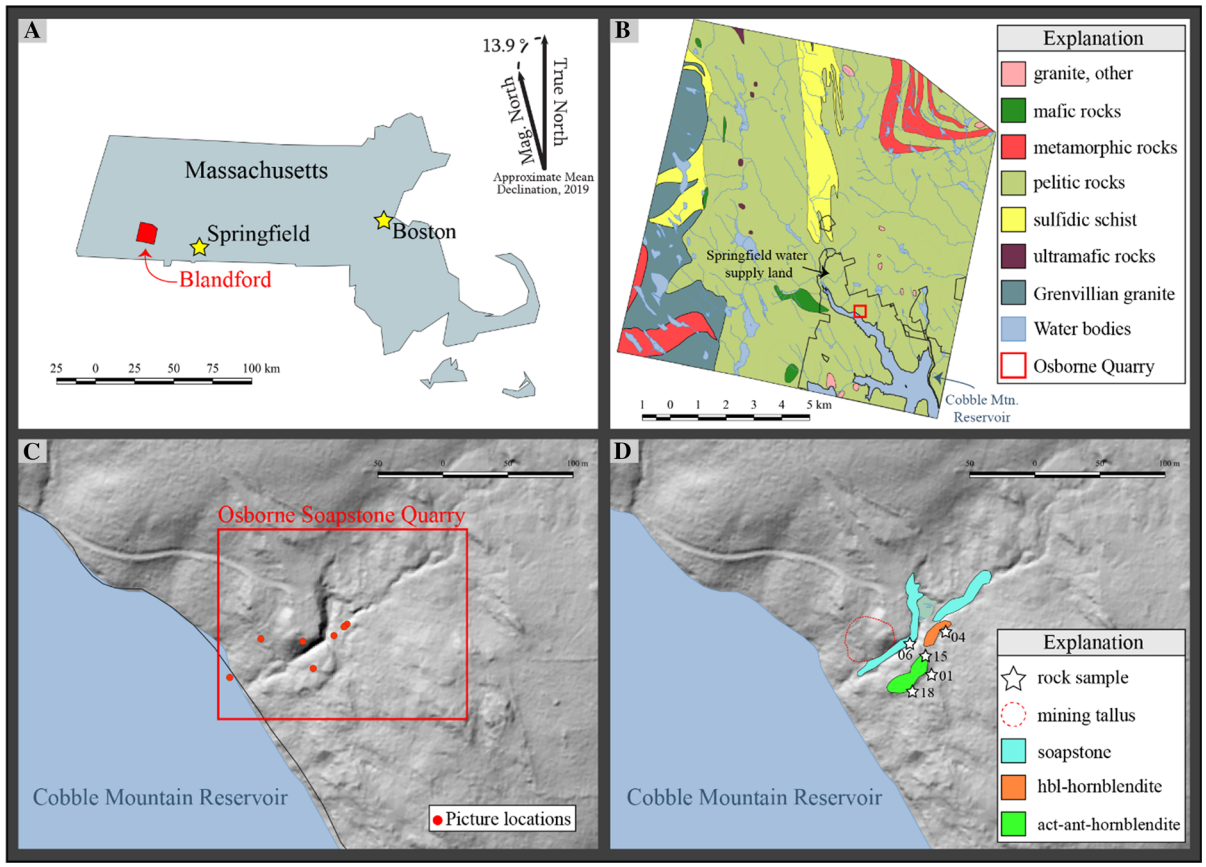

Fig. 1 **a** Regional context of study area, Blandford, MA, **b** bedrock geology of Blandford, MA, Springfield water supply land and the Osborne soapstone quarry are shown in the southeast, **c** Hillshade DEM of Osborne soapstone quarry area with picture locations (pictures available upon request) and **d** geologic outcrops, associated rock sample locations, and mining talus schematically illustrated atop hillshade. Note, outline for Osborne soapstone quarry is approximate. All GIS layers and data provided via MassGIS; terrain and LiDAR data provided via USGS and National Land Cover Database (NLCD); compiled in QGIS (shapefiles available upon request)

three generalized units featured within the locality: (1) soapstone: massive serpentine–talc, (2) interlayered chlorite schist and three-amphibole hornblendite, and (3) country rock (mica schist and amphibolite). In order to understand primary mineralogical sources of trace metals, samples of mafic and ultramafic schist were collected. Hand samples (10–30 cm in diameter) were also collected from talus, mine spoils, within stream channels, and within soil pits. Variably weathered samples were collected with the specific intent of observing the relationship between bulk weathering and mafic-to-ultramafic mineralogy in order to qualitatively assess the extent of trace metal-related phase alteration, breakdown, and redeposition.

Collected soil samples were weighed, air-dried at 25 °C to a constant mass, and sieved to < 2 mm. Nine soil pits were excavated upslope of the mine, within the mine, and below the mine (see Fig. 1 map) during June 2019. Soil pit locations were chosen to evaluate the impact of mine spoils on metal accumulation and mobility downslope. Upland locations, away from stream channels and hyporheic zones of streams, on convex microtopographic highs were sampled to avoid bias of hydric soils. Upslope soil pits were chosen to serve as control soils undisturbed by mining. Soil pits within the mine area were chosen to capture the impact of mining, particularly within mine spoils. Downslope soil pits were selected to capture near surface lateral transport of metals. First, 15 × 15 cm square sections of organic horizons were separated from the underlying mineral soil and collected. Second, a soil pit was excavated to 1 m depth or lithic contact and sampled

by each master horizon. Soils were oven-dried at 70 °C to a constant weight and sieved to < 2 mm.

Sediment grab samples of the top 10 cm were collected in ponding areas in June 2019 along a 70 m transect of the main stream that drains the catchment, which includes the former Osborne Soapstone Mine. Ponding areas were chosen to avoid oversampling coarse materials present in riffle areas and under sampling finer materials that are mobile under high discharge events. Six sediment samples were collected from upslope of the mine to capture incoming sediments from undisturbed soils. Six sediment samples were collected from the stream within the mine, which includes one of the open-pit trenches. Lastly, six sediment samples were collected downslope of the mine, prior to drainage into the Cobble Mountain Reservoir. Sediment samples were frozen at − 20 °C, freeze-dried to a constant mass, and sieved to < 2 mm.

Stream water was collected at six points along the main stream draining the catchment: two upslope, two within the mine area, and two downslope prior to entering the Cobble Mountain Reservoir. Samples were collected June 2019, during late spring as streams following the above average precipitation March to May 2019 and again at low base flow conditions mid-August 2019. One-liter acid-washed bottles and dip sampling method USGS protocols (Wilde and Radtke 1998) were used to sample stream waters at the six locations. Samples were stored on ice, measured for pH, and filtered to < 0.2 µm and acidified to pH 1.5 with trace metal-grade nitric acid. To concentrate samples for analysis by ICP-OES, samples were distilled from 1 L to 10 mL on a hot plate at 130 °C for 5 h within a closed fume hood.

Soil physicochemical analyses

Soil pH, texture, and %organic matter were measured for each soil horizon (Supplemental Table 1). For soil pH, a 2:5 soil−$CaCl_2$ solution (5 g soil to 12.5 g 0.1 M $CaCl_2$) was used. The $CaCl_2$ slurries were shaken for 1 h using a wrist-action shaker and vacuum extracted through a Whatman 40 filter. The pH of the extract was measured with a pH meter (8015 VWR). Loss-on-ignition was used to estimate % SOM, which is a simple and qualitative method but may overestimate organic matter content due to mineral dehydration and carbonates (Santisteban et al. 2004). To determine the percent loss-on-ignition, a 4-g air-dried subsample was combusted at 550 °C for 6 h. Soil texture was quantified using a modified Bouyoucos method with hydrometer readings taken at 60 s and 1.5 h after complete mixing of standard 1 L graduated columns (Gee and Bauder 1979; Jordan et al. 2019).

Bioavailable and strong acid extractions

Rock, soil, and sediment samples were subjected to bioavailable and strong acid extractions to determine their mobility and potential ecotoxicology for plants and animals. A modified Morgan extraction of 0.1 M ammonium acetate was used to quantify the bioavailable fraction of Cr, Co, Mn, Ni, and other metals. First, 2 g of soil was weighed into 50 mL centrifuge tube. 30 mL of 0.1 M ammonium acetate was added to each tube and shaken for 24 h. The slurry was subsequently centrifuged at 3000 rpm for 1 h, and the supernatant was decanted and filtered to < 0.45 µm. Bioavailable concentrations are given in Supplemental Table 2.

A strong acid digestion following USEPA method 3051A (USEPA 1996) was used to quantify extractable Cr, Co, Mn, Ni, and other metal concentrations through open-vessel digestion (Supplemental Table 3). Strong acid digestion was used instead of other operationally defined methods, to measure metals that are not within primary silicate mineral lattice and may become dissolved or biologically relevant within decades (Chen and Ma 1998). The digestion process used 1.0 g (± 0.1 g) of soil samples, digested with 5 mL of 9:1 ratio of trace metal-grade nitric acid to hydrochloric acid (15 M HNO3 + 10 M HCl, Fisher Scientific). The solution was heated to 80 °C for 45 min using a hot plate and diluted to 50 mL using 18.2 MΩ cm deionized water. For every 20 samples, a preparation blank and duplicate sample were included.

Extracts were further diluted using 18.2 MΩ cm deionized water and analyzed with an Agilent 5110 inductively coupled plasma-optical emission spectrometer (Agilent Technologies, Santa Clara, California, USA). Chromium, Co, Mn, Ni, and Fe concentrations in the preparation blank were < 0.1% of their respective measured concentrations, and all duplicates were within 15% CV. NIST Montana Soil 2711a standard reference material was also digested following this protocol, and recoveries were 85% for

Cr, 87% for Co, 85% for Mn, and 102% for Ni of their respected certified values (see Mackey et al. 2010).

Mineralogy and microscopy

Unoriented doubly polished thin sections were prepared from collected samples at the University of Massachusetts Amherst. Optical petrography, EDS phase mapping, and WDS full section electron compositional mapping were used to identify mineral assemblages and potential trace metal-bearing phases. EDS was also used to obtain quantitative data on mineral compositions and conducted with a beam current of 200.0 nA and voltage of 15 kV on a Zeiss Evo 50 scanning electron microscope (SEM). EDS hypermaps were collected using a single cycle pass. Compositional mapping of Mg Kα, Ni Kα, Mn Kα, and Cr Kα X-ray lines was conducted with a 35 μm step size, beam current of 200 nA, and voltage of 15 kV on the Cameca SX-100 electron microprobe. Trace metal (Ni, Mn, Cr) wavelength peaks were calibrated and refined on native metal standards using 2Θ fine peaking, verification, and appropriate shifting. SEM and electron probe analyses were conducted in the microanalysis facilities at the University of Massachusetts Amherst.

Total soil and mineral XRF analyses

Total concentrations of Co, Cr, Mn, Ni, and Fe in soils and rocks were determined using a X-200 XRF instrument from SciAps (SciAps Inc., Woburn, MA) (Supplemental Table 4). The X-200 utilizes three energy beams: 40 kV, 10 kV, and 50 kV, from an Rh anode alloy. For a detector, it uses a 20 mm 2-silicon drift detector and 135 eV resolution FWHM at 5.95Mn K-alpha line. Spectra were analyzed using Compton Normalization (EPA Method 6200).To account for inaccuracies in the software, data were further processed with a multi-element regression model developed from nine USGS rock standards (the additional four were BHVO-2, DNC-2, BIR-1, BCR-2, SBC-2, SDO-1, STM-2, GSP-2, W-2a) and one NIST standards (2711a) that use Cu, Zn, and Fe to improve accuracy of the measurements. For each rock hand sample, five different locations were measured with three spectra for each location. Soil samples were crushed to < 0.05 mm and packed into 7 mL polypropylene vessels lined with 6-μm-thick polyethylene terephthalate sheet, and the homogenized soil and sediment samples were measured once for 90s for the three energies. Total Cr, Co, Mn, Ni, and Fe concentrations were within 14% of their certified values, and duplicates were within 5% relative standard deviation for NIST 2711a.

Descriptive and statistical analyses

For soil comparisons, the three soil pits for each site were grouped together for each master soil horizon and again with all soil horizons together. In the soil and sediment comparisons, data were grouped together either by upslope, within mine, and downslope. Descriptive statistics were calculated in MATLAB. In-text mean values are given $\pm$ 1 standard error. Due to the limited sample sizes when comparing among soil pits horizons, rock samples, and sediments, nonparametric statistical tests were used: rank sign test and Kruskal–Wallis test.

Results and discussion

Mafic mineralogy and petrology

The mafic schist that confines the main body of exposed soapstone is subtly layered yet compositionally diverse. Closest to soapstone is a 3–5-m-thick layer of strongly foliated magnetite–chlorite schist, which sharply transitions into a 5–10-m-thick sequence of three-amphibole hornblendite. Iron-oxides are abundant and display a variety of morphologies, weathering textures, and trace metal relationships across these mafic lithologies. EDS analysis of Mg–Fe silicates and interstitial weathering-related sulfate phases indicates the presence of trace metals across all layers of mafic schist in the Osborne deposit.

The deposit-adjacent chlorite schist is comprised of strongly aligned equigranular plates of chlorite (clinochlore) that define microfolds and a prominent deformational fabric. Magnetite is common (up to 10% modally) and displays two morphologies. Oblong and amorphous magnetite are small (< 0.25 mm) and display weak alignment with the surrounding chlorite matrix. Euhedral magnetite up to 3 mm in diameter is dispersed throughout chlorite and commonly displays abundant microfractures infilled by chlorite. Large

magnetite crystals are often surrounded by disseminated subhedral flakes of ilmenite. EDS analysis of multiple ilmenite indicates the presence of trace quantities of Mn; compositions of phases in chlorite schist obtained by EDS acquisition are reported in Table 1.

Above the chlorite schist is interlayered asbestiform (actinolite + anthophyllite) and magnetite–ferrohornblende–hornblendite. Asbestiform hornblendite can display spectacular blades of actinolite and/or anthophyllite up to 7 cm in length (Fig. 2a). All three varieties of hornblendite contain up to 90% amphibole modally, with 5% chlorite and Fe-oxide, respectively. Asbestiform hornblendite (Fig. 2b, c) is typically massive and is comprised of aggregates of radiating euhedral blades of actinolite and anthophyllite. Actinolite and anthophyllite are rarely seen coexisting in thin section; modally, the asbestiform hornblendite is up to 85% actinolite (or anthophyllite), 10% chlorite, and 5% accessory phases (magnetite, ilmenite, biotite). Ferrohornblende–hornblendite (Fig. 2d) consists of strongly foliated euhedral ferrohornblende and interstitial subhedral magnetite. Ferrohornblende is small (< 2 mm), equigranular, pale-to-dark green, and strongly pleochroic. Collected samples of weathered hornblendite, both from spoils and outcrop, contain localized zones of extensive grain-margin degradation in amphibole and chlorite. Alteration products appear as either rusty overgrowths, likely goethite or limonite (Fig. 2e), or silicified (quartz) rims up to 5 μm wide (Fig. 3c). Matrix chlorite analyzed with EDS contains Ni (Fig. 2f) and may serve as local trace metal sorption surfaces within a relatively non-adhesive amphibole matrix (Butt and Cluzel 2013).

Small inclusions of magnetite up to 2 mm diameter are found in all varieties of hornblendite. Magnetite displays considerable morphological differences with weathering. In fresh hornblendite, subhedral grains are found between amphibole or as inclusions in amphibole and chlorite. Amorphous magnetite is common in weathered hornblendite (Fig. 3a) and appears as lobate < 250 μm globs adjacent to microfracture networks in actinolite. Quantitative EDS analysis and high-resolution phase mapping (hypermaps) indicate the presence of small (< 10 μm) euhedral phases concentrated in Cr, Mn, and Co adjacent to amorphous magnetite (Fig. 3b). These phases are interpreted to be weathering-related precipitates that may have been deposited as a consequence of submicron scale inter-actinolite fluid flow. Phases of similar compositions are found in close association with weathered actinolite and contained additional trace metals such as Ni and Ag (Fig. 3c, d). EDS acquired compositions of amorphous magnetite and interstitial trace metal precipitates are reported in Table 1.

Ultramafic mineralogy and petrology

The main working at the former Osborne Quarry is a massive exposure of serpentine–talc. Modally, this soapstone is 45% talc, 40 serpentine (chrysotile), 5% biotite, 5% magnetite, and < 5% accessory phase (anthophyllite, chlorite). The matrix is comprised of intergrown talc and fibrous serpentine (chrysotile). Morphologically variable magnetite porphyroclasts occur in cross-cutting 2 mm wide veinlets of biotite (Fig. 4a through d). Magnetite also occurs as fine (submicron) inclusions in talc and is commonly intergrown with serpentine. Serpentine is highly acicular, up to 2 cm long, less than a 2 mm wide, displays weak pale-green pleochroism, and often occurs in radiating masses or as pseudomorphs after

Table 1 EDS compositions of amorphous magnetite (Fig. 3a, b) and interstitial trace metal-bearing phase (Fig. 3b) in weathering hornblendite, Os-18

Magnetite			Trace metal phase		
Element	Atom Wt. %	Error	Element	Atom Wt. %	Error
EDS cation analysis, Os-18: weathered actinolite–hornblendite					
O	62.94	13.69	O	64.03	11.42
Fe	32.06	5.95	Si	18.04	1.74
Mn	1.26	0.41	Ni	5.62	1.19
Cr	3.74	0.78	Ag	9.55	2.64
			S	2.75	0.36

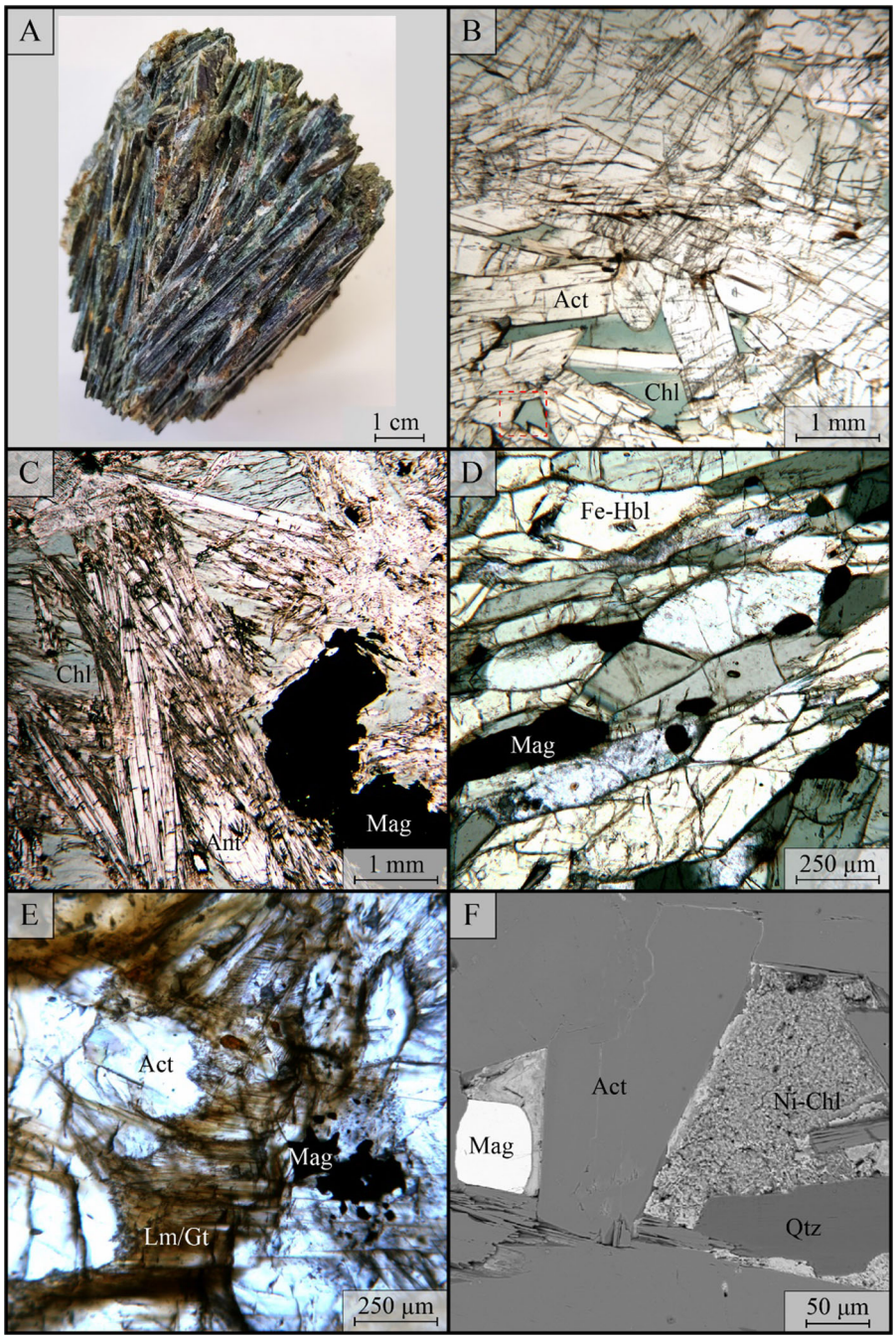

Fig. 2 **a** Spectacular actinolite in hand sample. Plane-polarized light (PPL) micrographs of **b** fresh actinolite–hornblendite, sample Os-01, **c** fresh anthophyllite–hornblendite, sample Os-15, **d** fresh ferrohornblende–hornblendite, sample Os-04, **e** alteration products along weathered actinolite grain boundary, sample Os-18, **f** backscatter electron (BSE) image of Ni chlorite and magnetite in fresh hornblendite, sample Os-01. Mineral abbreviations: *Act* actinolite, *Chl* chlorite, *Ant* anthophyllite, *Mag* magnetite, *Fe-Hbl* ferrohornblende, *Lm* limonite, *Gt* goethite, *Qtz* quartz

anthophyllite. Talc exhibits rusty discoloration in fresh soapstone and is overgrown by limonite and/or goethite in weathered rinds (Fig. 4e, f). Weathering-related alteration products (limonite and goethite) occur throughout even fresh soapstone, commonly as

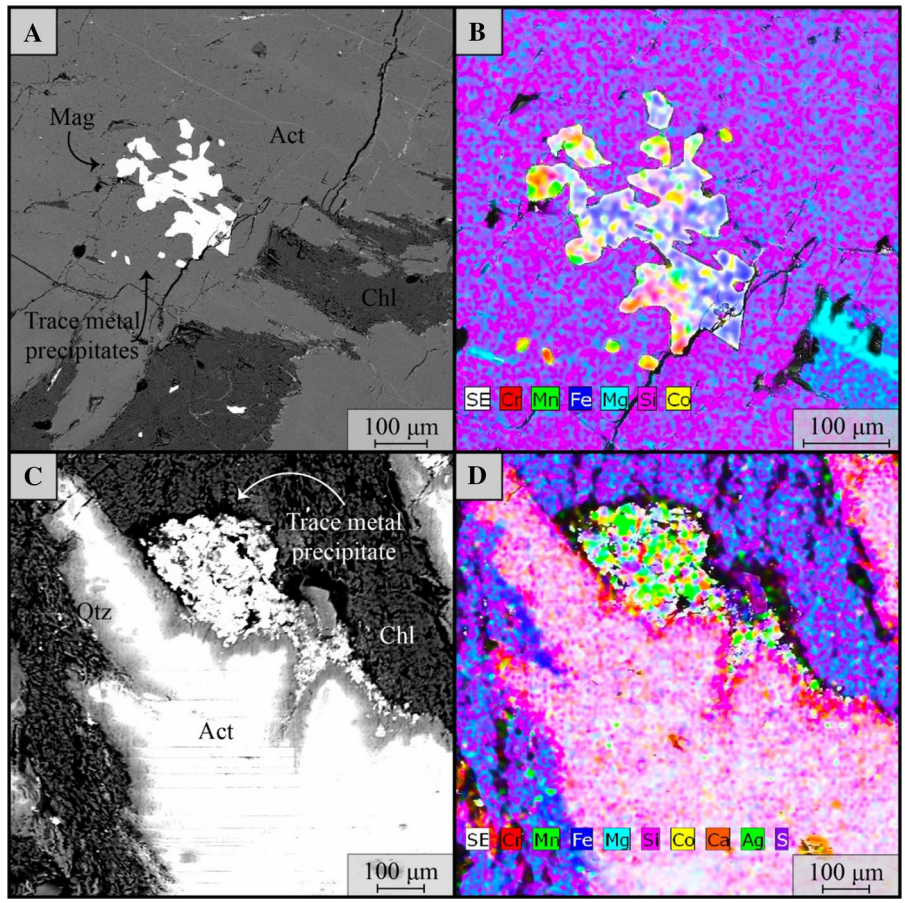

Fig. 3 Sample Os-18, weathered actinolite–hornblendite, **a** BSE image and **b** EDS hypermap of amorphous magnetite and surrounding trace metal precipitates in microfractured actinolite and chlorite matrix. **c** BSE image and **d** EDS hypermap of weathered actinolite displaying quartz overgrowth along grain boundary. Mineral abbreviations: *Act* actinolite, *Chl* chlorite, *Mag* magnetite, *Qtz* quartz. BSE imaging and EDS acquisition conducted through 20 nm carbon (graphite) coat, beam current and voltage of 200 nA and 15 kV, and tilt angle = 0

overgrowths on talc or within discrete intergranular fractures.

Total, bioavailable, and strong acid rock extractions

Total concentrations of Cr, Co, Mn, and Ni were evaluated with XRF analysis in hand samples of chlorite schist, serpentine–talc, and hornblendite. Chromium concentrations were significantly higher in the serpentine–talc (4041 ± 420 mg kg^{-1}) compared to the chlorite schist (545 ± 246 mg kg^{-1}) and hornblendite (70 ± 10 mg kg^{-1}). Cobalt concentrations were also higher in the serpentine–talc (444 ± 25 mg kg^{-1}) compared to the chlorite schist (230 ± 93 mg kg^{-1}) and hornblendite (28 ± 6 mg kg^{-1}). Nickel concentrations were highest in the chlorite schist (4052 ± 1370 mg kg^{-1}) but also elevated in the serpentine–talc (1824 ± 240 mg kg^{-1}) and within typical crustal rock concentrations for the hornblendite (12 ± 1 mg kg^{-1}). Manganese concentrations were comparable for the chlorite schist (1387 ± 336 mg kg^{-1}), serpentine–talc (904 ± 182 mg kg^{-1}), and hornblendite (1009 ± 250 mg kg^{-1}). These results show that the mafic and ultramafic compositions determined here are comparable to other ultramafic bodies globally and reveal their ability to host significantly elevated concentrations of Cr, Cu, and Ni within talc, magnetite inclusions, and amorphous inclusions.

To determine the mobility of elements from the rock samples to the surrounding soils, sediment, and

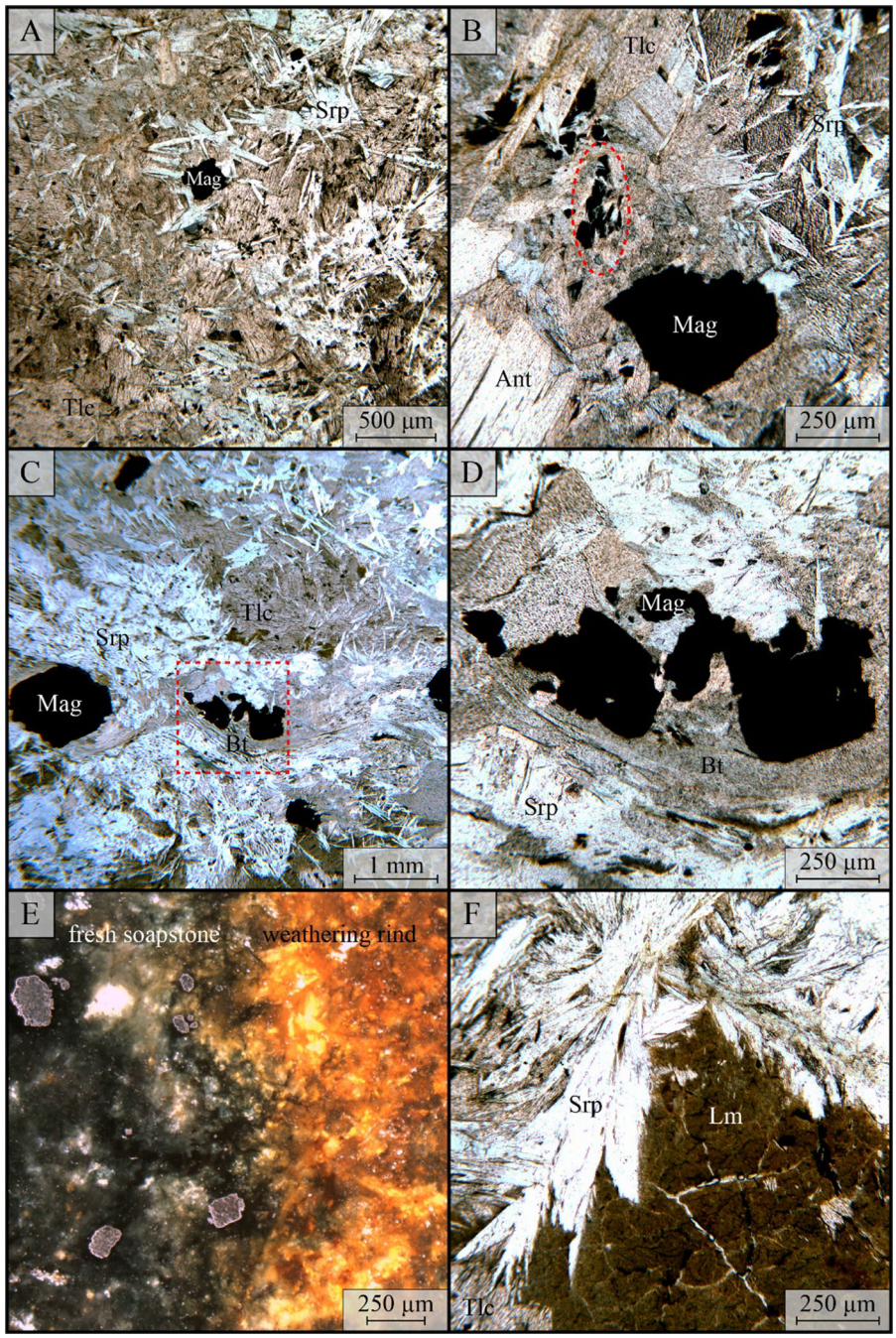

Fig. 4 Photomicrographs of main soapstone deposit at Osborne, sample Os-02, **a** in PPL, primary ultramafic mineral assemblage in main soapstone deposit, fibrous serpentine, massive talc with fine magnetite inclusions, and subhedral magnetite porphyroclasts; **b** intergrown serpentine and magnetite (in red circle) and relict anthophyllite (lower left); **c** euhedral-to-subhedral magnetite porphyroblasts surrounded by biotite; **d** 4x-zoom of red box in **c**; **e** reflected polarized light (RPL) photomicrograph of weathering rind; **f** limonite-after-talc intergrown with serpentine. Mineral abbreviations: *Srp* serpentine, *Tlc* talc, *Mag* magnetite, *Ant* anthophyllite, *Bt* biotite, *Lm* limonite

reservoir, ground subsamples of chlorite schist, serpentine–talc, and hornblendite were extracted for bioavailable and strong acid concentrations of Cr, Mn, Ni, and Co. Bioavailable Cr and Co concentrations were < 0.1 mg kg^{-1} for all three rocks, while bioavailable Ni concentrations ranged from 0.02 to 0.94 mg kg^{-1} (Fig. 5). Bioavailable Mn concentrations ranged from 0.7 to 1.8 mg kg^{-1} (Fig. 5). These bioavailable concentrations are $< 1\%$ of their respective total concentrations. This extraction demonstrates that although total concentrations are significantly elevated, the risk of immediate bioavailability and transport as dissolved species is very low from this ultramafic deposit.

Strong acid extractions were also carried out to estimate the fraction of metals not within silicates, but the portion that may become mobilized with further chemical weathering. Strong acid extractable Cr and Co concentrations ranged from 0.1 to 34 mg kg^{-1} for all three rocks, while strong acid extractable Mn and Ni concentrations ranged from 2 to 162 mg kg^{-1} (Fig. 5). These strong acid extractions were $< 5\%$ of their respective total concentrations, further demonstrating that the trace metals within the mafic and ultramafic rock are held within insoluble silicate and Fe-oxide forms.

Soil and sediment physicochemical properties

The soils throughout the area within and surrounding the mine are typical secondary growth forest soils. Organic matter concentrations were highest in the A horizons and decreased with depth (Supplemental Table 1). This increase in soil pH with increase in depth from the surface is typical in mine waste soils and is restricted to the mine drainage area which can be attributed to the alkaline ultramafic parent rock and accumulation of organic matter in upper horizons (Dinelli and Tateo 2001). Similarly, acidity was greatest in A horizons with pH values 3.8 to 4.4 and decreased with depth in BC horizons with pH values of 4.5 to 4.9 (Supplemental Table 1). Soils were dominated by sand (75 to 86%). Some silt (12 to 20%) and limited amounts of clay (2–5%) were characterized as

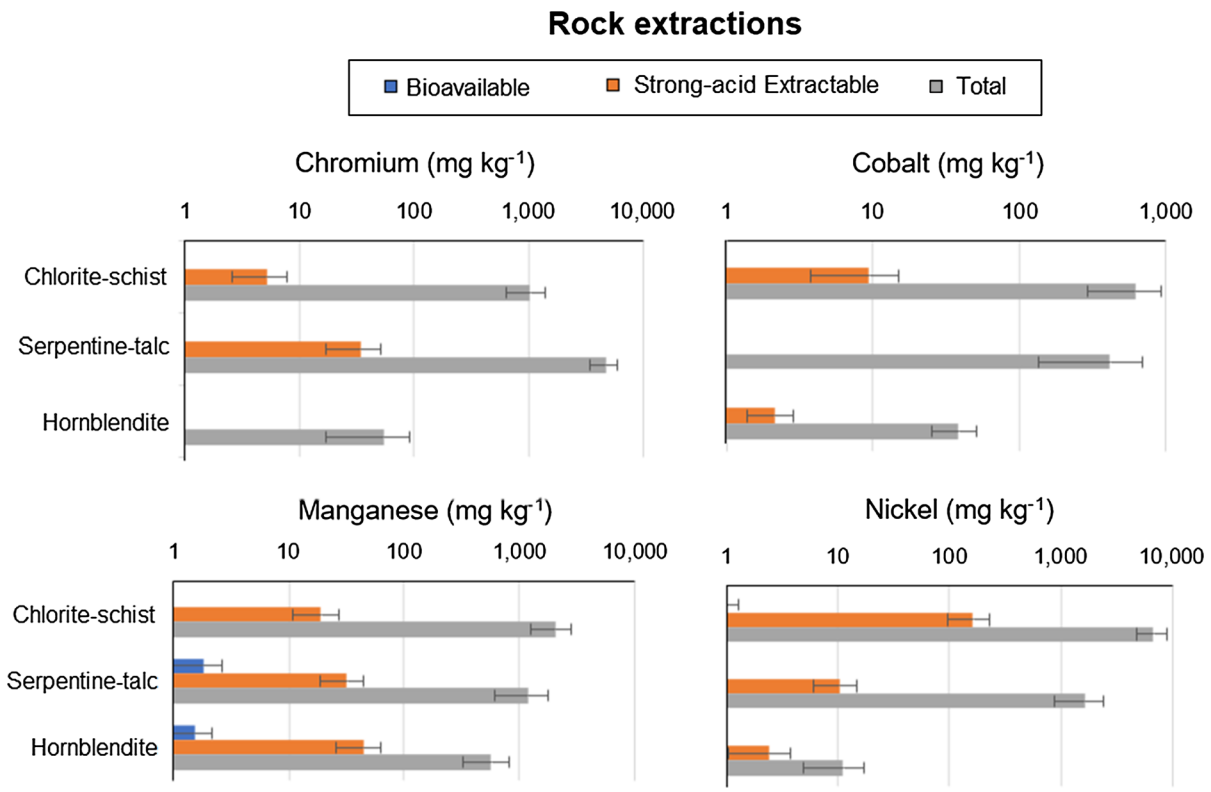

Fig. 5 Extractability of Cr, Mn, Ni, and Co from rock samples from within mine outcrops and walls. $N = 4$ for each rock sample and error bars are $\pm$ 1 standard deviation

sandy loams or loam sand textures. The high sand content and in turn low water holding capacity are typical of soils derived from serpentine bedrock (Robinson et al. 1996). Soil organic matter, soil pH, and particle size were not significantly different among the three landscape positions (Supplemental Table 1).

Sediments were collected as grab samples of the top 10 cm from pool areas along the two main streams draining the mine trench and mine spoils. Sediments upslope had higher organic matter content (7.9%) and greater acidity (pH 5.4) compared to sediment within the mine (2.1% and pH 5.8) and downslope positions (2.4% and pH 5.6) (Supplemental Table 1). Particle size distribution of sediment was dominated by sand (93 to 97%), but upslope positions had a greater proportion of silt (4%) compared to within the mine (3%) and downslope (1%) (Supplemental Table 1).

Total, bioavailable, and strong acid extractable soil and sediment extractions

Soils upslope, within mine, and downslope positions were studied of the mine to determine their metal concentrations and if they are potentially mobile or bioavailable phases. Overall total soils concentrations for Cr (119 ± 12 mg kg^{-1}), Ni (65 ± 10 mg kg^{-1}), and Co (73 ± 11 mg kg^{-1}) were elevated above typical background soil concentration for Cr $\sim$ 40 mg kg^{-1}, Ni $\sim$ 20 mg kg^{-1}, and Co $\sim$ 20 mg kg^{-1} (Adriano 2001; Kabata-Pendias 2015) (Fig. 6; Supplemental Table 4). Overall total Mn concentration (894 ± 11 mg kg^{-1}) was comparable to background soil Mn concentrations of $\sim$ 1000 mg kg^{-1} (Adriano 2001) (Fig. 6; Supplemental Table 4). Soil A horizons in upslope positions had lower Cr, Co, Mn, and Ni, than within mine and downslope soils. Moreover, B and BC horizons in upslope positions had lower Mn, Ni, and Co concentrations than within mine and downslope positions. These results suggest that the soils within the mine areas and downslope are enriched in Mn, Ni, and Co from the mafic and ultramafic rock with inconclusive soil enrichment of Cr due to the mine, potentially natural weathering of additional Cr sources upslope.

Sediment samples from the primary stream that drains the mine area were collected to determine whether sediment transport is an important pathway for trace metal export from the mine. Total sediment concentrations of Cr, Ni, and Co were less than or comparable to their respective total soil concentrations, but total sediment Mn was significantly higher than soil concentrations (Supplemental Table 4; Figs. 5 and 6). Sediment concentrations of Cr, Mn, and Ni were above typical background soil concentrations stated above (Adriano 2001; Kabata-Pendias and Mukherjee 2007). Total sediments concentrations of Cr, Mn, and Ni were similar upslope of the mining activity compared to downslope positions (Supplemental Table 4; Fig. 6). These results suggest that transport of metals from mine spoils and the mine face as sediments is a limited export pathway, as upslope sediment transport has similar metal concentrations.

Bioavailable soil and sediment concentrations of Cr, Mn, Ni, and Co were several orders of magnitude lower than their respective total concentrations. Bioavailable Mn concentrations ranged from 0.2 to 20.2 mg kg^{-1} (Supplemental Table 2; Figs. 6 and 7). Bioavailable Cr, Ni, and Co soil concentrations were < 0.3 mg kg^{-1} (Supplemental Table 2; Figs. 6 and 7). Moreover, when bioavailable Cr, Ni, and Co concentrations were compared as a percent of their total concentrations, their bioavailable fraction was $<$ 0.5%. These results highlight that although total concentrations are elevated to typical soils and sediments, bioavailability is very low for plant uptake or ingestion from terrestrial organisms.

Strong acid extractable soil and sediment concentrations of Cr, Mn, Ni, and Co were constituted a larger proportion of their respective total concentration, ranging from 5 to 79% (Supplemental Table 3). Strong acid extractable Mn soil and sediment concentrations ranged from 28 to 528 mg kg^{-1} and comprised between 8 and 37% of the total Mn concentrations (Supplemental Table 3; Figs. 6 and 7). Higher soil strong acid extractable Mn concentrations occurred within mine A horizons but were comparable for B and BC horizons (Supplemental Table 3). However, sediment Mn concentrations were greatest in upslope positions compared to within mine and downslope positions (Supplemental Table 3, Fig. 5). Strong acid extractable Cr soil and sediment concentrations were 3 to 39 mg kg^{-1} and ranged from 10 to 42% of the total Cr concentration (Supplemental Table 3; Figs. 6 and 7). Strong acid extractable Cr concentrations were the greatest upslope and within mine soils (Supplemental Table 3). Lastly, strong acid extractable Ni and Co concentrations were 1 to 29 mg kg^{-1} and ranged from

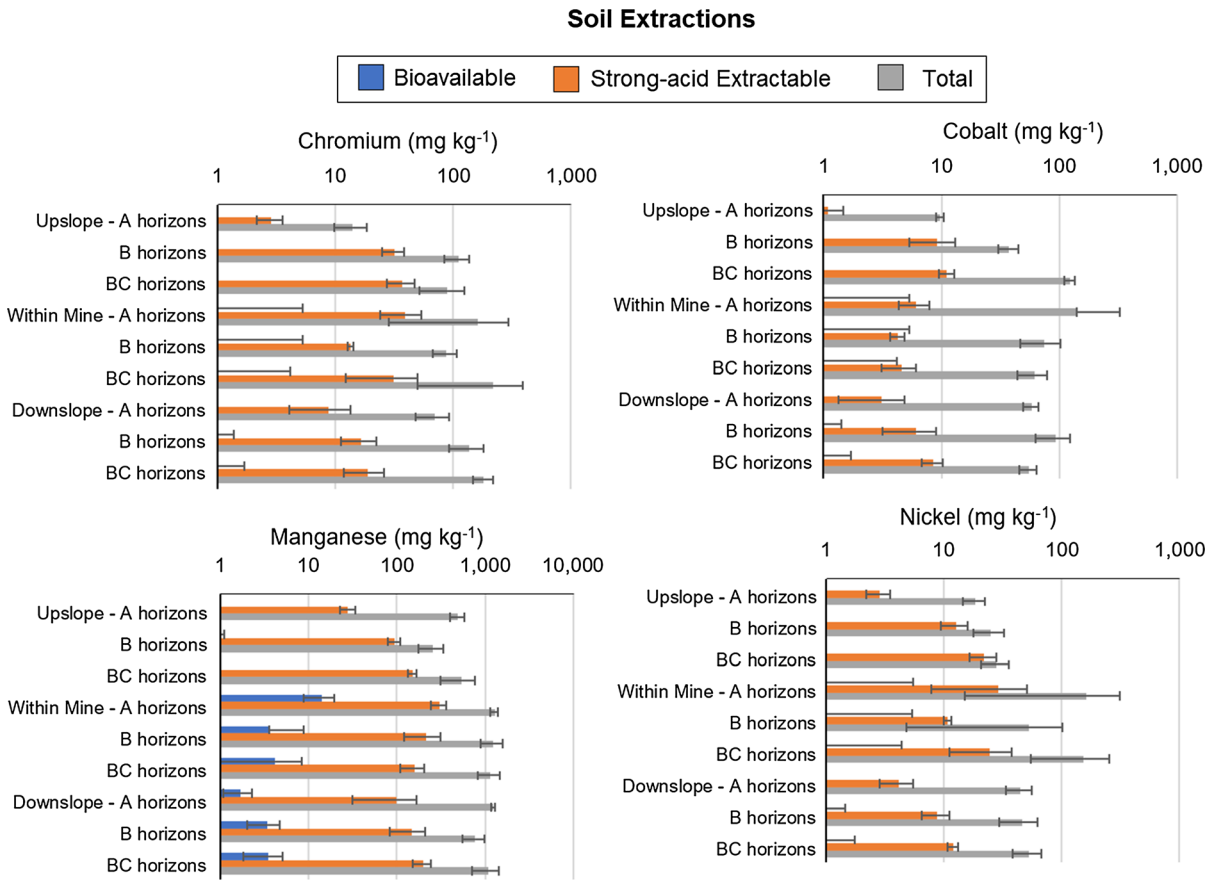

Fig. 6 Extractability of Cr, Mn, Ni, and Co from soil samples upslope, within, and downslope of the mine. $N = 3$ for each horizon and error bars are ± 1 standard deviation

6 to 79% and 4 to 25% of their total concentrations, respectively (Supplemental Table 3). These results highlight that strong acid extractable concentrations of Cr, Co, Mn, and Ni are important fractions of their total respective concentrations. Thus, substantial portions of these metals (up to 37% for Mn, 42% for Cr, 79% for Ni) were not within crystalline silicate minerals, but either adsorbed or within secondary oxides, complexed with organic compounds, or in highly weathered silicates. Previous research found shows exchangeable Mn concentrations are higher at lower pH and Eh levels in soils (Agnieszka and Barbara 2012); thus, the greater dissolution of Mn occurred at lower redox potential may be driving the higher amounts of bioavailable Mn in the soils (Adriano 2001). These results suggest that these metals are susceptible to mobilization through intensive acidic weathering (Fig. 8). However, the strong acid concentrations are comparable to typical soil concentrations (Adriano 2001) and not many orders of magnitude greater.

Cr, Mn, Ni, and Co stream water

Stream water results show increases in Cr, Co, Mn, and Ni concentrations within the mine areas under both high and low flow conditions; demonstrating they are leaching from the mine spoils of the mine. Stream water Mn and Ni concentrations show they are affected by concentration-discharge rates, as high flow had significantly lower concentrations than under low flow conditions near base discharge rates. Most importantly, however, all stream water concentrations were below drinking water standards. Stream water Cr concentrations were far below USEPA primary drinking water standards of 100 µg L^{-1}, and Mn concentrations were below but approaching USEPA secondary drinking water standard of 50 µg L^{-1}

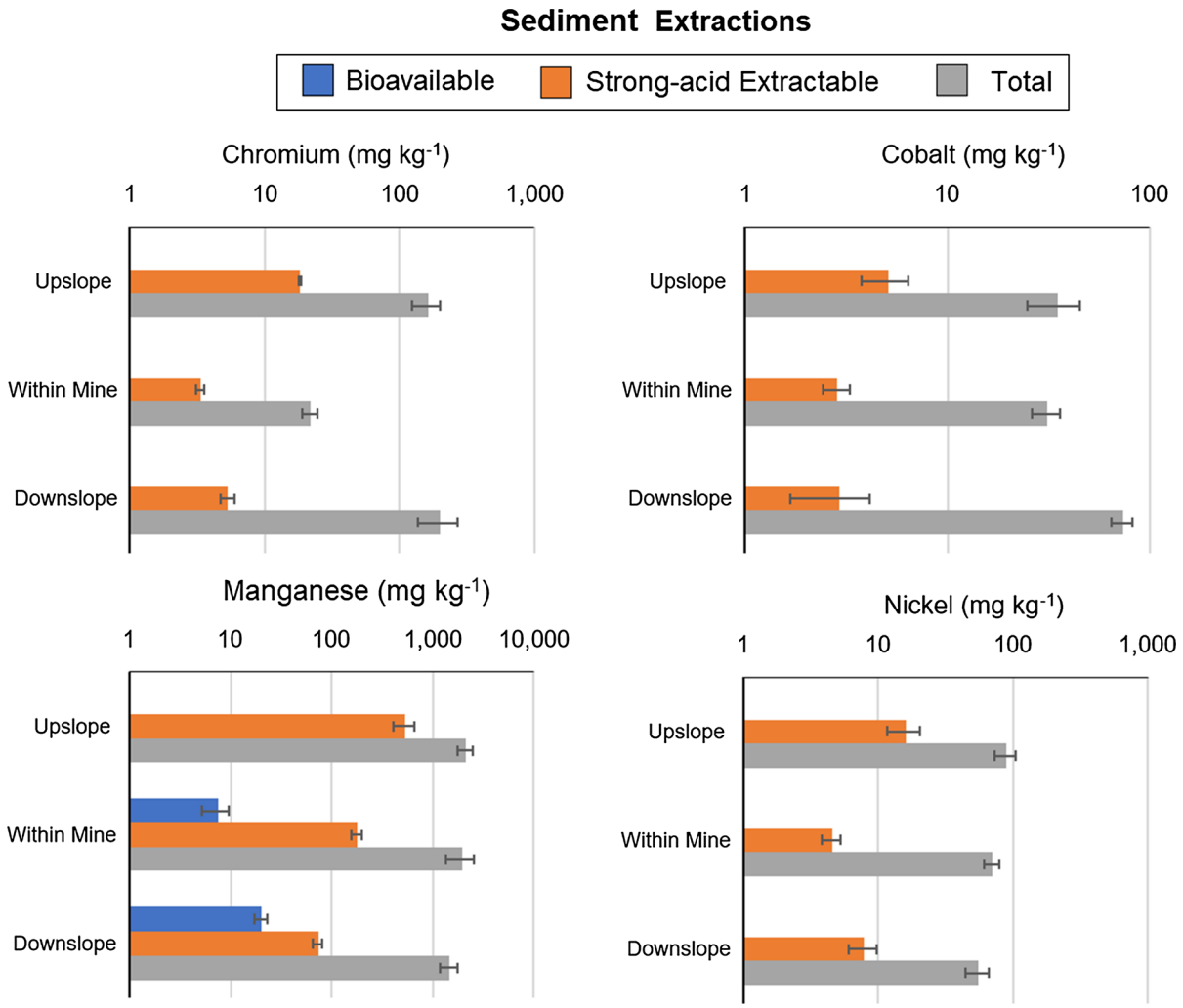

Fig. 7 Extractability of Cr, Mn, Ni, and Co from sediment samples upslope, within, and downslope of the mine. $N = 6$ for location and error bars are ± 1 standard deviation

(Fig. 7; USEPA 2019a, b). Stream water concentrations of Ni were below but approaching WHO drinking water guideline of 70 µg L^{-1}. The low Cr stream water concentrations were likely due to sorption and immobilization by secondary Fe and Mn oxides, which has been observed to be a dominant process in Cr sorption in many previous studies (e.g., Feng et al. 2006). Cobalt and Ni may also be adsorbed to Mn and Fe oxides, but to a lesser extent than Cr (Ma and Hooda 2010). We hypothesize further that Mn and Ni, which had the highest stream water concentrations, may be mobilized by chelation with dissolved organic compounds (see Scott et al. 2002). Scott et al. (2002) had similar observations from Mn-rich stream water in which dissolved organic matter-rich, reduced waters mobilized Mn to stream water, but Mn precipitated out during stream transport.

Synthesis and conclusions

The former Osborne Quarry is a layered 3–5-m-thick deposit of ultramafic serpentine–talc–soapstone with marginal mafic schist including a three-amphibole hornblendite within meters of one of Massachusetts' largest freshwater reserves. The mafic-to-ultramafic mineralogy observed throughout the deposit can be characterized by abundant Fe–Mg phyllosilicates and

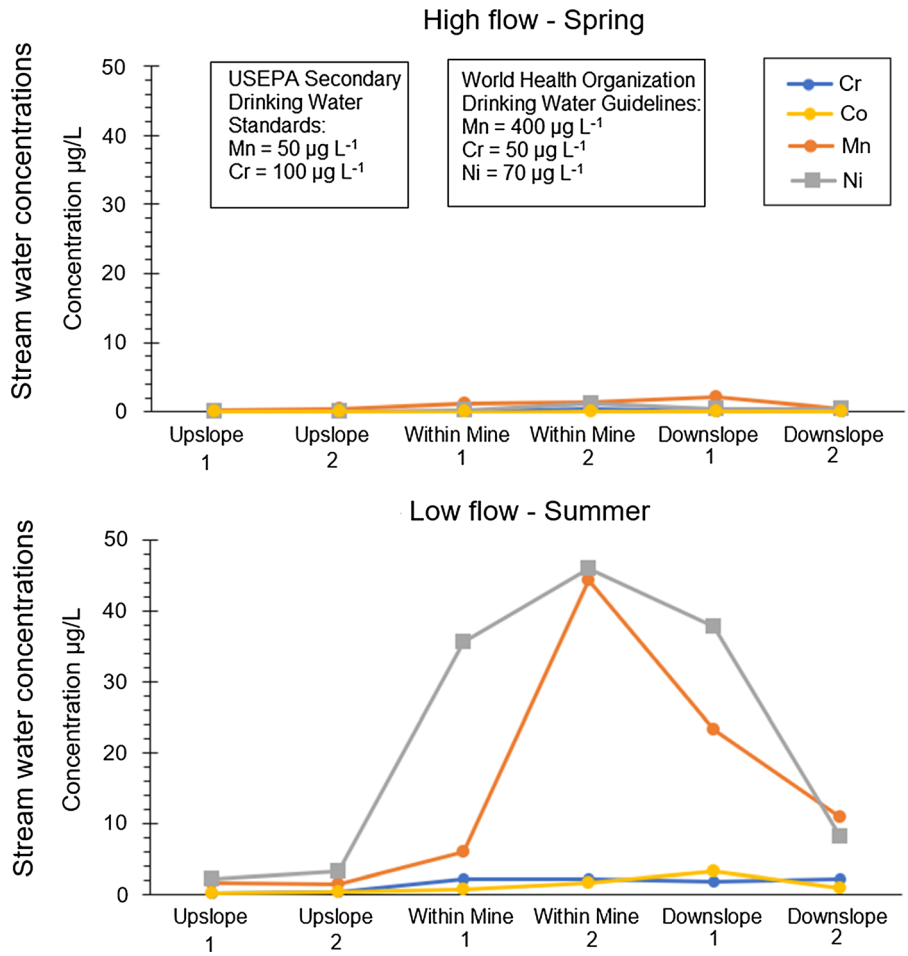

Fig. 8 Stream water concentrations of Mn, Cr, and Ni collected June 2019 along the main flow path from upslope, within, and downslope of the mine area (WHO (2017) and USEPA (2019a, b)). Cobalt was below detection limits

primary Fe-oxides. The primary Fe-oxides display numerous morphologies as seemingly dictated by mineralogical setting and weathering susceptibility. EDS compositional observation of weathered and non-weathered sheet silicates indicates the presence of Ni, thereby suggesting that ultramafic minerals in former mining exposures can be important host phases for trace metals, as observed in many other laterite deposits (Butt and Cluzel 2013; Wei et al. 2019).

The high concentration of trace metals, including Cr, Mn, and Co, within weathered amphibole and accessory grains of amorphous magnetite suggests that weathering of exposed mafic and ultramafic mine spoils and faces may exert a strong local control on trace metal release to subsurface soil horizons and stream waters. Talc may be especially problematic due to its inherent fissile nature, which promotes grain splitting and surface area expansion, which ultimately may increase potential trace metal release. Sediments and soils show limited bioavailability demonstrating negligible imminent hazardous for terrestrial ecosystems and the reservoir. However, strong acid concentrations suggest further weathering will release more Mn, Co, and Ni to soils and surface waters. Stream water concentrations were below secondary drinking water standards. Even though Mn and Ni concentrations approach drinking water standards, it was under low flow conditions when stream water discharge was lowest, approximately < 1 L per second. The former Osborne Quarry is not a highgrade laterite deposit, but its proximity to local freshwater sources and Fe–Mg rich mineral assemblages make it a unique case site to address potential feedbacks between bedrock geology,

trace metal mobility, and vulnerability of drinking water quality.

Acknowledgements We thank the Springfield City Water and Sewer Commission for granting permission to study the former Osborne Mine. We are grateful to Lawrence Bull and Kenneth Gliesman for their guidance and knowledge of the mine and its minerals. This research was supported by funding to Dr. Justin Richardson from the University of Massachusetts Amherst.

References

Adriano, D. C. (2001). *Arsenic*. Springer, New York, NY: In Trace elements in terrestrial environments.

Agnieszka, J., & Barbara, G. (2012). Chromium, nickel and vanadium mobility in soils derived from fluvioglacial sands. *Journal of Hazardous Materials, 237*, 315–322.

Avudainayagam, S., Megharaj, M., Owens, G., Kookana, R. S., Chittleborough, D., & Naidu, R. (2003). Chemistry of chromium in soils with emphasis on tannery waste sites. *Reviews of environmental contamination and toxicology* (pp. 53–91). New York, NY: Springer.

Babula, P., Adam, V., Opatrilova, R., Zehnalek, J., Havel, L., & Kizek, R. (2008). Uncommon heavy metals, metalloids and their plant toxicity: A review. *Environmental Chemical Letter, 6*, 189–213.

Bradley, D. W. (1983). Tectonics of the Acadian orogeny in New England and adjacent Canada. *Journal of Geology, 91*, 381–400.

Butt, C. M. B., & Cluzel, D. (2013). Nickel laterite ore deposits: Weathered serpentinites. *Elements, 9*(2), 123–128.

Cenni, E., Bussotti, F., & Galeotti, L. (1998). The decline of a Pinus nigra Arn reforestation stand on a limestone substrate: The role of nutritional factors examined by means of foliar diagnosis. *Annales des sciences forestières, 55*(5), 567–576.

Chen, M., & Ma, L. Q. (1998). Comparison of four USEPA digestion methods for trace metal analysis using certified and Florida soils. *Journal of Environmental Quality*, *27*(6), 1294–1300.

Chute, N. E. (1969). The talc, soapstone, and asbestos deposits of Massachusetts. *USGS Open File Report*, 1–48.

Da Silva, J. F., & Williams, R. J. P. (2001). *The biological chemistry of the elements: the inorganic chemistry of life*. Oxford: Oxford University Press.

de Varennes, A., Carneiro, J. P., & Goss, M. J. (2001). Characterization of manganese toxicity in two species of annual medics. *Journal of Plant Nutrition, 24*(12), 1947–1955.

Dinelli, E., & Tateo, F. (2001). Sheet silicates as effective carriers of heavy metals in the ophiolitic mine area of Vigonzano (northern Italy). *Mineralogical Magazine*, *65*(1), 121–132.

Emerson, B. K. (1898). *Geology of Old Hampshire County, Massachusetts, comprising Franklin, Hampshire, and Hampden Counties* (p. 29). Geological Survey: U.S.

Feng, X. H., Zhai, L. M., Tan, W. F., Zhao, W., Liu, F., & He, J. Z. (2006). The controlling effect of pH on oxidation of Cr (III) by manganese oxide minerals. *Journal of Colloid and Interface Science, 298*(1), 258–266.

Gasser, U. G., Juchler, S. J., Sticher, H., & Hobson, W. A. (1995). The fate of chromium and nickel in subalpine soils derived from serpentinite. *Canadian Journal of Soil Science, 75*(2), 187–195.

Gee, G. W., & Bauder, J. W. (1979). Particle size analysis by hydrometer: a simplified method for routine textural analysis and a sensitivity test of measurement parameters 1. *Soil Science Society of America Journal, 43*(5), 1004–1007.

Haynes, E. N., Sucharew, H., Kuhnell, P., Alden, J., Barnas, M., Wright, R. O., et al. (2015). Manganese exposure and neurocognitive outcomes in rural school-age children: The communities actively researching exposure study (Ohio, USA). *Environmental Health Perspectives, 123*(10), 1066–1071.

Hitchcock, E. (1833). *Report on the geology, mineralogy, botany, and zoology of Massachusetts*: Amherst, Massachusetts.

Izbicki, J. A., Ball, J. W., Bullen, T. D., & Sutley, S. J. (2008). Chromium, chromium isotopes and selected trace elements, western Mojave Desert, USA. *Applied Geochemistry, 23*(5), 1325–1352.

Jordan, J., Cernak, R. S., & Richardson, J. B. (2019). Exploring the role of soil geochemistry on Mn and Ca uptake on 75-year-old mine spoils in western Massachusetts, USA. *Environmental Geochemistry and Health*, 1–13.

Kabata-Pendias, A. (2015). *Trace elements in abiotic and biotic environments*. CRC Press.

Kabata-Pendias, A., & Mukherjee, A. B. (2007). *Trace elements from soil to human*. Berlin: Springer.

Leyssens, L., Vinck, B., Van Der Straeten, C., Wuyts, F., & Maes, L. (2017). Cobalt toxicity in humans—A review of the potential sources and systemic health effects. *Toxicology, 387*, 43–56.

Li, H. F., Gray, C., Mico, C., Zhao, F. J., & McGrath, S. P. (2009). Phytotoxicity and bioavailability of cobalt to plants in a range of soils. *Chemosphere, 75*(7), 979–986.

Ma, Y., & Hooda, P. S. (2010). Chromium, nickel and cobalt. *Trace Elements in Soils, 13*, 461–480.

Mackey, E. A., Christopher, S. J., Lindstrom, R. M., Long, S. E., Marlow, A. F., Murphy, K. E., et al. (2711a). Certification of three NIST renewal soil standard reference materials for element content: SRM 2709a San Joaquin Soil, SRM 2710a Montana Soil I, and SRM 2711a Montana Soil II. *NIST Special Publication, 260*(172), 1–39.

Oze, C., Fendorf, S., Bird, D. K., & Coleman, R. G. (2004). Chromium geochemistry of serpentine soils. *International Geology Review, 46*(2), 97–126.

Oze, C., Bird, D. K., & Fendorf, S. (2007). Genesis of hexavalent chromium from natural sources in soil and groundwater. *Proceedings of the National Academy of Sciences, 104*(16), 6544–6549.

Proenza, J. A., Lewis, J. F., Galí, S., Tauler, E., Labrador, M., Melgarejo, J. C., et al. (2008). Garnierite mineralization from Falcondo Ni-laterite deposit (Dominican Republic). *Revista de la Sociedad Española de mineralogía, 9*, 197–198.

Rabenhorst, M. C., Foss, J. E., & Fanning, D. S. (1982). Genesis of Maryland soils formed from serpentinite. *Soil Science Society of America Journal, 46*(3), 607–616.

Raous, S., Echevarria, G., Sterckeman, T., Hanna, K., Martins, E. S., & Becquer, T. (2013). Potentially toxic metals in ultramafic mining materials: Identification of the main bearing and reactive phases. *Geoderma, 192*, 111–119.

Ratié, G., Jouvin, D., Garnier, J., Rouxel, O., Miska, S., Guimarães, E., et al. (2015). Nickel isotope fractionation during tropical weathering of ultramafic rocks. *Chemical Geology, 402*, 68–76.

Robinson, B. H., Brooks, R. R., Kirkman, J. H., Gregg, P. E. H., & Gremigni, P. (1996). Plant-available elements in soils and their influence on the vegetation over ultramafic ("serpentine") rocks in New Zealand. *Journal of the Royal Society of New Zealand*, *26*(4), 457–468.

Santisteban, J., Mediavilla, R., López-Pamo, E., Dabrio, C., Zapata, M., García, M., et al. (2004). Loss on ignition: A qualitative or quantitative method for organic matter and carbonate mineral content in sediments? *Journal of Paleolimnology*, *32*(3), 287–299.

Schwertmann, U., & Latham, M. (1986). Properties of iron oxides in some New Caledonian oxisols. *Geoderma, 39*(2), 105–123.

Scott, D. T., McKnight, D. M., Voelker, B. M., & Hrncir, D. C. (2002). Redox processes controlling manganese fate and transport in a mountain stream. *Environmental Science & Technology, 36*(3), 453–459.

Singh, H. P., Mahajan, P., Kaur, S., Batish, D. R., & Kohli, R. K. (2013). Chromium toxicity and tolerance in plants. *Environmental Chemistry Letters, 11*(3), 229–254.

Tracy, R. J., Robinson, P., & Wolff, R. A. (1984). Metamorphosed ultramafic rocks in the Bronson Hill Anticlinorium, Central Massachusetts. *American Journal of Science, 284*, 530–558.

U.S. Census Bureau 2019. Quick Facts: United States. https://www.census.gov/quickfacts/fact/table/US/ PST045218. Retrieved October 2, 2019.

USEPA. 1996. "Method 3050B: Acid digestion of sediments, sludges, and soils," Revision 2. Washington, DC.

USEPA United States Environmental Protection Agency Secondary Drinking Water Regulations: Guidance for Nuisance Chemicals. https://www.epa.gov/dwstandardsregulations/secondary-drinking-water-standards-guidance-nuisance-chemicals. Retrieved Accessed July 9, 2019.

USEPA United States Environmental Protection Agency National Primary Drinking Water Regulations: Guidance for Nuisance Chemicals. https://www.epa.gov/ground-water-and-drinking-water/national-primary-drinking-water-regulations. Retrieved July 9, 2019.

Wei, F., Feng, Y., Luo, P., Zhang, Y., Huang, X., Zeng, X., et al. (2019). Weathering of ophiolite remnant and formation of Ni Laterite in a strong uplifted Tectonic Region (Yuanjiang, Southwest China). *Minerals*, *9*(1), 51.

Wilde, F.D., & Radtke, D.B. (eds.) (1998). *Handbooks for water-resources investigations: National field manual for the collection of water-quality data*. US Geological Survey.

World Health Organization. (2017). *Guidelines for drinking-water quality: fourth edition incorporating the first addendum*. Geneva: Licence: CC BY-NC-SA 3.0 IGO.

Zen, E.-A., Goldsmith, R., Ratcliffe, N. M., Robinson, P., Stanley, R. S., Hatch, N. L., Jr., Shride, A. F., Weed, E. G. A., & Wones, D. R. (1983). Bedrock geologic map of Massachusetts: U.S. Geological Survey, Reston, VA, scale 1: 250,000.